Materials & Design 227 (2023) 111695

Contents lists available at ScienceDirect

Materials & Design

journal homepage: www.elsevier.com/locate/matdes

Multi-Scale tailoring of lithium ion diffusion from densification to coarsening

Sujin Park [a], Janghyuk Moon [b], Seongwan Jang [a], Haitao Zhang [c], Chang-Jun Bae [a,*]

[a] Department of 3D Printing Materials, Powder Materials Division, Korea Institute of Materials Science, Changwon, Gyeongnam 51508, Republic of Korea
[b] School of Energy Systems Engineering, Chung-Ang University, Heukseok-Ro, Dongjak-Gu, Seoul 06974, Republic of Korea
[c] CAS Key Laboratory of Green Process and Engineering, Beijing Key Laboratory of Ionic Liquids Clean Process, Institute of Process Engineering, Chinese Academy of Sciences, Beijing 100190 China

HIGHLIGHTS

- Facilitation mechanisms of lithium ion diffusion were investigated through thermal stability, grain growth kinetics, and diffusion model.
- Oxygen evolution and destruction of the layered structure were prohibited by thermal treatment at 1100 °C, securing stable lithium ion diffusion at micro-level.
- High capacity retention of 96.5 % was achieved at 1C by controlled densification and coarsening based on the kinetic study of grain growth at macro -level.
- The electrochemical properties showed good agreement with our developed diffusion model, suggesting the strategic way to achieve lower tortuosity and higher diffusion coefficient by controlling rapid grain growth.

GRAPHICAL ABSTRACT

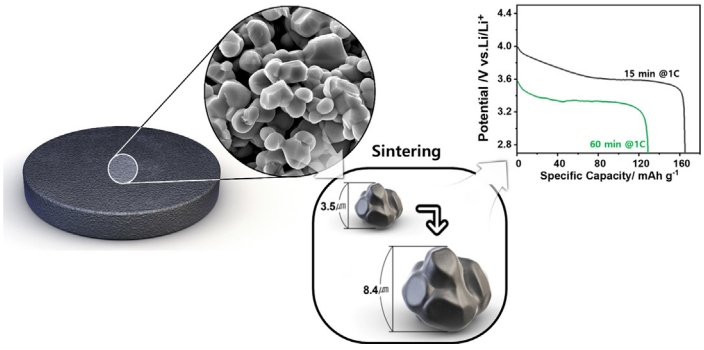

ARTICLE INFO

Article history:
Received 14 October 2022
Revised 30 January 2023
Accepted 3 February 2023
Available online 4 February 2023

Keywords:
Lithium ion batteries
Highly energy densified electrode
Multi-Scale Tailoring
Densification
Coarsening
Li-diffusion

ABSTRACT

The performance of lithium-ion batteries is highly dependent on the morphology of the grain and structure of the electrode, which can be optimized for either high power or high energy. Despite the progress in all-solid-state batteries, the behavior of densification and coarsening has not yet been investigated on cathode. Herein, we investigated the strategies how to manipulate Li-ion diffusion at the different dimensions of micro- to macro level, facilitating the diffusion as tailoring the multi-scale path from densification to coarsening. First, the influence of microstructure on tortuosity and diffusivity was studied to understand the effect of sintering. Increased sintering time was expected to deteriorate electrochemical properties owing to lower diffusivity, and higher tortuosity. Second, the grain growth and densification behavior were studied in conjunction with the critical temperature for multi-scale tailoring without significant thermal degradation. At longer sintering times, densification was sluggish and had a monotonous increment of 2.5 %/h. However, the grain sizes greatly increased to 8.37 μm, leading isolated pores breaking. Finally, the tailored diffusivity and tortuosity were compared with the calculated results to

* Corresponding author.
E-mail address: baecj01@kims.re.kr (C.-J. Bae).

https://doi.org/10.1016/j.matdes.2023.111695

understand intra- and inter-diffusion. Our finding provides clues to facilitate the diffusion of Li-ion by controlled densification and coarsening behavior in highly densified electrode.

1. Introduction

Lithium ion batteries (LIBs) have long played an important role in energy storage systems; however, its safety related issues continue to receive increased scrutiny and are viewed as an intrinsic problem that needs to be resolved [1,2]. All-solid-state batteries (ASSBs), with inflammable inorganic electrolytes and highly densified electrodes, have been developed as ideal solutions for high safety [3,4]. Given the various processes for fabricating ASSBs, sintering cathodes, in particular, have many benefits. These include their high density and mechanical properties, as well as their applications in energy storage devices such as multifunctional electrodes, micro-batteries, and thick electrodes for ultra-high energy density. In the past decade, several studies have attempted to fabricate engineered electrodes by sintering, such as co-sintering the cathode with a solid electrolyte and spark plasma sintering [5]. However, densification behavior of cathodes has not yet been investigated, and it is necessary to understand the effect of densification and coarsening on electrochemical performance [6,7]. The most popular material used in sintered is $LiCoO_2$ (LCO), which has higher electrical conductivity. However, it has limited relative density (up to 60 %) and needs to be improved [8]. In addition, the thermal stability of the cathode is another issue to prevents significant degradation during heat treatment. The strategy to obtain a densified sintered electrode with fast Li-ion diffusion should consider both the effect of grain growth on Li ion diffusion at the macro level and thermal degradation at the micro level.

At the macro level, understanding the sintering behavior is the key factor in tailoring the electrochemical properties and influencing the intercalation and transport of Li ions [9]. In general, large grains lower the diffusivity by reducing the number of grain boundaries and longer diffusion paths in the bulk. The diffusion in grain boundaries has low migration barriers with a high concentration of diffusion-mediating defects, where the diffusivity of the grain boundary is 10^3–10^4 faster than that of the grain [10,11]. Therefore, small grains without coarsening are preferred for fast Li-ion diffusion, thereby enabling grain growth to be controlled along with the activation energy during sintering. Sintering of the cathode material can be categorized into three stages: initial neck growth, densification, and coarsening [12]. Among these, the second stage of densification is the beginning of densification and coarsening. This results in rapid sintering, which has an extensive impact on Li-ion diffusion given the magnitude of the grain size and density. Despite the scope for further investigation, studies on the correlation between Li-ion diffusion and microstructures along with different sintering environments have yet to be published to the best of our knowledge.

At the micro level, cathode degradation has been reported at high temperatures during synthesis, local oxygen evolution, and cation mixing [13]. Oxygen release leads to the formation of electrochemically inactive Co_3O_4 as a cathode with a local phase transition from a layered structure to spinel and then to a rock salt structure, which deteriorates the electrochemical performance [14,15]. Cation mixing is another issue that degrades electrochemical properties. [16,17]. The migration of transition-metal ions to the Li layer changes the equilibrium Li slab distance, thus increasing the activation barrier for diffusion [18]. Consequently, many approaches have been attempted to avoid transition metal (TM) migration through surface coating, cation doping, and changing stacking sequences [19]. Although various efforts have been made to mitigate oxygen release and cation mixing during the synthesis process, understanding the thermal degradation at the electrode level during sintering has never been investigated.

In this study, we report a highly densified LCO fabricated in various sintering environments by studying the sintering kinetics, activation energy for grain growth to design diffusivity, and diffusion length. To secure stable Li-ion diffusion without thermal degradation, we investigated its thermal and structural stability, revealing the oxygen evolution and destruction of the layered structure at the critical point of 1154 °C. In addition, the fast diffusion rate was achieved without rapid grain growth based on the kinetic study to design densified electrode. Finally, the electrochemical performance was intensively studied to shed light on the correlation between the microstructures and Li-ion diffusion. The properties showed good agreement with our calculated results, indicating longer diffusion path and reduced number of grain boundaries for the main rate-limiting parameters degrading the fast diffusion at a high C-rate of 1C. Comparing with the previous studies on densified cathode, our work firstly not only supply densification and coarsening behavior with kinetic study, but also supply a strategy way to design tailorable electrode without thermal degradation.

2. Experimental procedure

2.1. Fabrication of sintered electrodes

LCO powder (Nippon Chemical Industrial, Japan) and Super P (MTI Korea, Korea) were used to prepare pellet electrodes. Super P was intentionally added to fabricate an artificial pathway for Li ions, eliminated around 600 °C in ambient atmosphere, and turned into a porous structure. The acrylate-based curable resin was prepared using trimethylopropane triacrylate (TMPTA, Sigma-Aldrich) and 2,2′-Azobis (2-methylbutyronitrile) (AIBN, Junsei) as the monomer and thermal initiator, respectively. To prepare the sintered electrode, LCO and Super P, at a ratio of LCO:Super P = 80:10, were homogeneously mixed for 2 min at 2000 rpm using a mixer (Thinky, Japan) for pre-mix of dry powder. Subsequently, the curable resin with 3 wt% AIBN as the thermal initiator was added to the mixture and mixed for 10 min at 1000 rpm. Next, 2-propanol (acrylate resin:2-propanol = 4:1 w/w) was added as an additional solvent to lower the viscosity for homogenous mixing. In addition, 2-propanol was evaporated at 55 °C for 2 h in a vacuum oven. The dried mixed powder was placed in a stainless-steel die (10 mm diameter) and pressed under a pressure of 2 MPa for 30 s. The prepared pellets were cured at 120 °C for the cross-linked binder and then sintered at a ramp rate of 4 °C/min from 25 °C to 1100 °C in an ambient atmosphere. During sintering, the prepared pellets were surrounded by sacrificial LCO bed powder to prevent the evaporation of cobalt. The sintered electrodes were polished to a thickness of 150 μm for electrochemical testing.

2.2. Characterization of sintered electrodes

A simultaneous thermal analyzer-mass spectrometer (STA-MS, STA 409 PC/QMS 403C, NETZSCH) was used on pure LCO using flowing air at a heating rate of 4 °C min^{-1}. The phase transformation depending on the sintering temperature was confirmed by X-ray diffraction (XRD, Max-2500VL, Rigaku) using Cu Kα radiation at

1°/min for 2θ from 10 °to 80°. The morphologies and microstructures were characterized using scanning electron microscopy (SEM, JSM-6610LV, JEOL). The densities of the sintered pellets were measured using Archimedes' technique. The polished sintered electrodes were electrochemically tested against lithium foil electrodes in coin cells (CR2032) assembled in an Ar-filled glove box. Two layers of separator (Wellcos Corp., 2320, Korea) and a liquid electrolyte that consisted of 1.0 M LiPF6 in the ratio EC: DEC = 1:1 were used. The galvanostatic charge–discharge tests of sintered electrodes were conducted in a voltage range of 2.7–4.2 V vs Li/Li^+ using a battery cycler (Battery Cycle System, WBCS 3000, Won A Tech. Co.). First, for the first cycle to form a stable solid electrolyte interphase (SEI) layer, the cells were galvanostatically charged to 4.2 V at 0.1C rate, maintained at 4.2 V until the current decreased to a rate of 0.02C, and then discharged to 2.7 V vs Li/Li^+. The discharge capacities were calculated based on active material loading. For the GITT experiments, current of 0.1C was applied for 5 min, then cells were allowed to relax for 25 min. These procedures were repeated until the cut-off voltage of 4.2 V.

2.3. Model development

The categorization of diffusion pathways in the sintered electrode was simplified as follows: diffusion in the crystal, diffusion from one primary to another, and diffusion within pores filled with electrolytes. As a significant phase transformation was not detected and was well-maintained, the structure of LCO was observed, which can be considered negligible with respect to the diffusion in the crystal. Thus, diffusion from one primary to another and from the electrode to the pore was considered to reveal the rate-limiting parameters. The modified Bruggeman relationship was applied to calculate the effective diffusion length.

$$\tau = \gamma\varepsilon^{-\frac{1}{2}} \tag{1}$$

where τ is the tortuosity, γ is equal to 1.5 when sintered ceramics have porosity of 0.15–0.5, and ε is the porosity at different sintering times. Given Eq. (1), the effective diffusion length of L_{eff} can then be determined as:

$$L_{eff} = T \cdot \gamma\varepsilon^{-\frac{1}{2}} \tag{2}$$

where T is the thickness of the sintered electrodes. Note that L_{eff} represents the diffusion within the pores in the sintered electrode. The diffusion length of lithium ions was calculated using Fick's law.

$$L_{eff} = \sqrt{Dt} \tag{3}$$

where D is the effective diffusivity and t is the diffusion time. Furthermore, diffusion from one grain boundary to another was considered to be the ratio of diffusivity between the grain boundary and bulk. The diffusivity of D_{eff} for different sintering times can be derived as follows:

$$D_{eff} = D_{g.b} \cdot X_{g.b} + D_b \cdot X_b \tag{4}$$

where $D_{g.b}$ and D_b are the diffusivities of the grain boundary and grain, respectively, and $X_{g.b}$ and X_b indicate the fractions of grain boundaries and grains in the sintered electrode, respectively. The value of $D_{g.b}$ has been reported to be 10^3–10^4 times higher than that of D_b [10]. Based on this, the diffusivities of the grain were measured by GITT method and the diffusivity of grain boundary were assumed to be 10^{-10} cm^2/sec, which is reasonable for LCO [11].

The diffusivity of the liquid electrolyte was not considered in this calculation because the ionic conductivity was 10^3–10^4 times higher than that of LCO, which cannot be the limiting parameter for considering diffusion.

3. Results and discussion

3.1. Effect of densification and coarsening on Li-diffusion

Lithium cobalt oxide (LCO) must be sintered to obtain a highly densified electrode. However, the effect of sintering on the diffusion path and diffusivity has not yet been studied, and therefore, needs to be studied to tailor the electrochemical properties in terms of the application prospects, such as energy storage systems (ESS), mobiles, or power tools. To better understand the sintered electrode, the diffusion pathways are categorized as follows, as shown in Fig. 1: diffusion in the crystal, diffusion from one primary to another, and diffusion into pores [20]. Diffusion within the grain is directly related to grain growth and diffusion in the grain boundary, whereas solid electrolytes refer to tortuosity. For instance, larger grains caused by rapid grain growth during sintering result in longer diffusion lengths in the bulk. In addition, increased electrode density due to densification leads to increased interfacial resistance due to the reduced electrolyte-filled pores and higher tortuosity following the Bruggeman relationship of $\tau = \gamma\varepsilon^{-\frac{1}{2}}$.

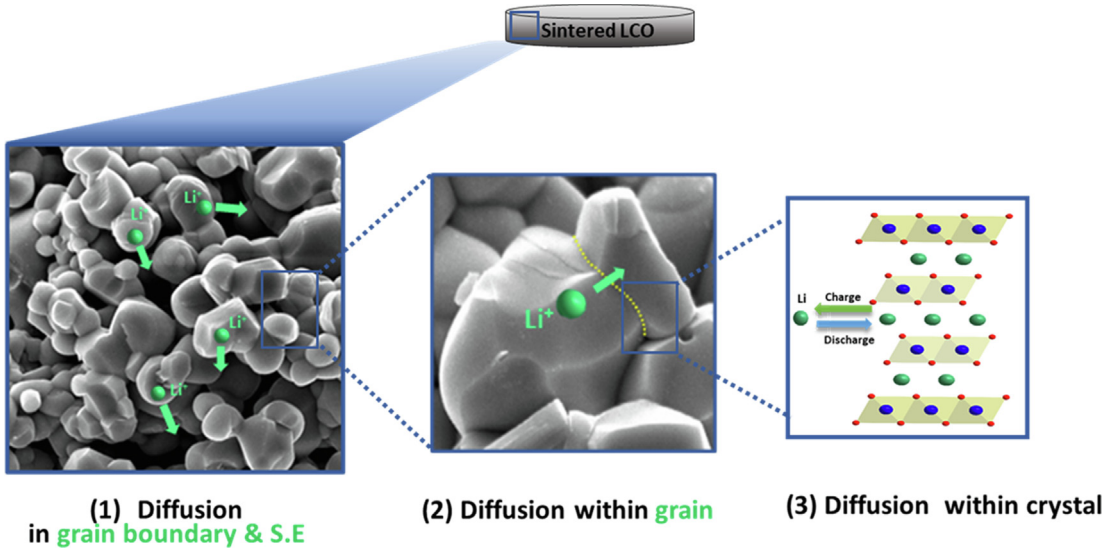

Fig. 1. Schematic representation for the diffusion mechanism of sintered electrode; diffusion in grain boundary and solid electrolytes, within grain and within crystal.

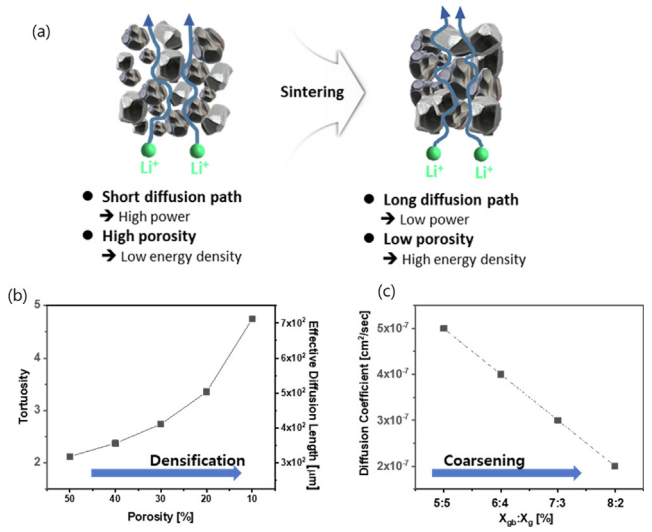

Fig. 2. (a) Schematic representation for the effect of densification and coarsening on electrochemical properties, effect of (b) porosity on diffusion length and (c) fraction of grain boundary and grain on diffusion coefficient.

A schematic comparison of densification and coarsening before and after sintering is shown in Fig. 2a. Before sintering, the electrode exhibited a comparatively short diffusion path owing to the small grain size. However, a long and tortuous path can be found after sintering with low porosity, thus leading to a higher energy density and slow diffusion. Hence, tortuosity and grain size were used for the calculation, and the parameters for the diffusion model are tabulated in Fig. 2a and 2b. Given an electrode thickness of 150 μm, the effective diffusion length depends on the tortuosity at different porosities. An increased sintering time or temperature will reduce the porosity, giving rise to an escalated tortuosity from 2.12 to 4.74, thus leading to longer diffusion lengths. Additionally, grain growth is considered to be the effective diffusivity (D_{eff}) at a fraction of grain boundaries and grains in the sintered electrode. D_{eff} is expected to decrease from 5.0×10^{-7} to 2.0×10^{-7} cm2/*sec* as bigger grain size reduces the number of grain boundaries. The performance of the densified electrode can be tailored based on the expected electrochemical parameters, which are affected by the porosity and grain size. Therefore, microstructure tailoring is discussed in the next section to secure stable and fast diffusion without thermal degradation.

3.2. Thermal and structural stability of sintered LCO electrode

There are several thermal degradations that should be resolved, as shown in Fig. 3: oxygen evolution, cation mixing, and coarsening. The thermal stability of the sintered LCO electrode was investigated using weight loss as a function of temperature up to 1400 °C, as shown in Fig. 4a. A weight loss of 3 % and an endothermic reaction were simultaneously detected at around 1154 °C. The loss and reaction, which are matched with the temperature of all outgassing curves at 16 and 32 AMU in Fig. 4b, indicate the event of oxygen gas evolution. When oxygen evolved from the LCO electrode at approximately 1150 °C, the destruction of the layered structure occurred as follows: [15].

$LiCoO_2 \rightarrow 1/(2\text{-}y)\ Li_yCo_{2-y}O_2 + (1\text{-}y)/(2\text{-}y)\ Li_2O + (1\text{-}y)/(2\text{-}y)\ 1/2O_2$.

The main weight loss, starting from 1120 °C to 1170 °C, resulted from the evaporation of lithium oxide and oxygen, leading to a nonstoichiometric phase of $Li_yCo_{2-y}O_2$ ($y < 1$) and a detrimental

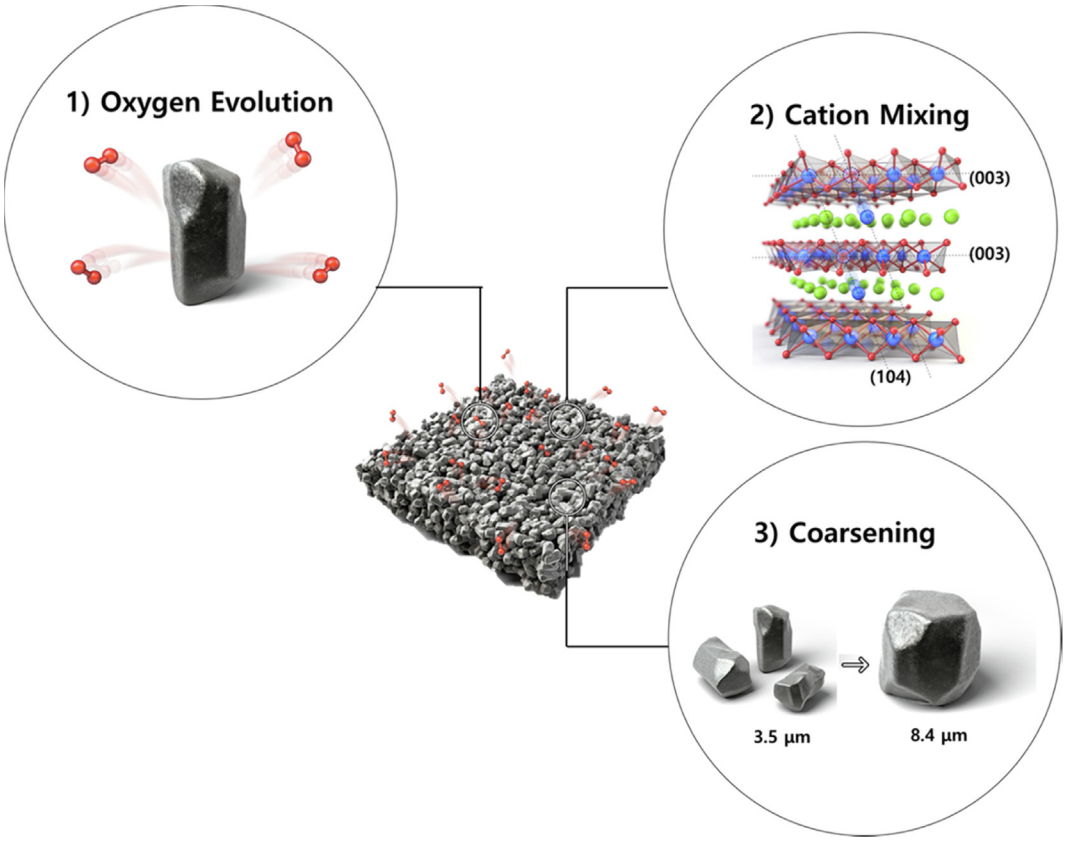

Fig. 3. Schematic representation for degradation of $LiCoO_2$ at high temperature.

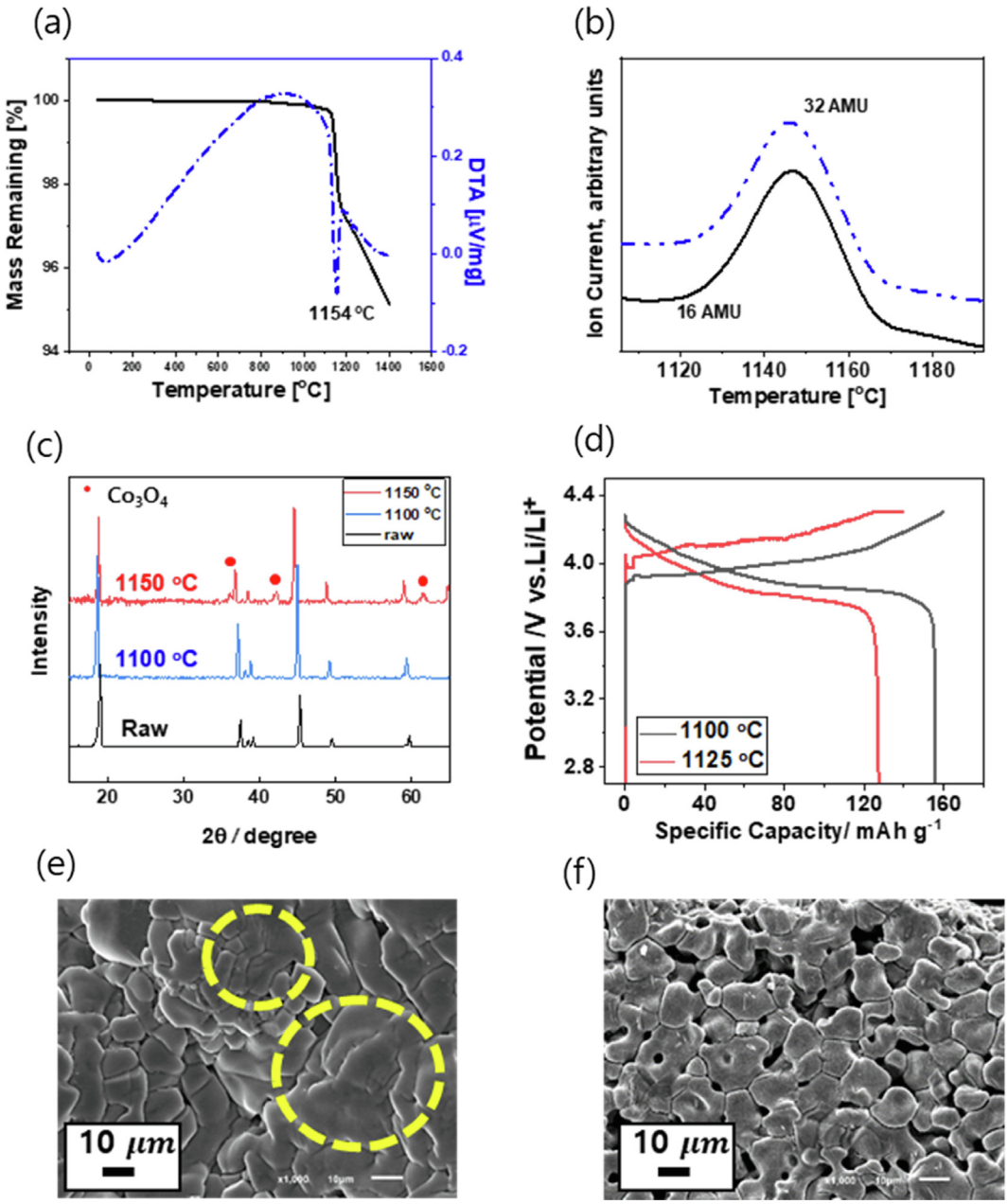

Fig. 4. Thermal properties of LCO (a) Thermogravimetric at different temperature revealing decomposition at 1154 °C, (b) Evolution of oxygen gas, (c) X-ray diffraction patterns showing formation of Co_3O_4, (d) Comparison of electrochemical performance sintered at 1100 °C and 1125 °C and (e,f) SEM images of LCO sintered at 1150 °C and 1100 °C, respectively.

effect on the electrochemical properties by reducing the amount of lithium.

Fig. 4c shows the XRD diffraction peaks of the electrodes sintered at the different temperatures of 1100 and 1150 °C for 240 min. The electrodes sintered at 1150 °C not only include the main peaks of LCO (003) and (101) at two thetas of 18 and 45, but also new diffraction peaks of Co_3O_4 at two thetas of 36, 42, and 61, undergoing thermal degradation from unstable nonstoichiometric $Li_yCo_{2-y}O_2$ ($y < 1$) to CoO, and finally transformed to Co_3O_4 during cooling. This is evidence of the destroyed layered structure confirmed using XRD analysis.

$$Li_yCo_{2-y}O_2 \rightarrow yLiCoO_2 + 2(1\text{-}y)CoO$$

However, the electrode sintered at 1100 °C displays the same diffraction patterns before and after thermal treatment, which is identical to that of the raw LCO powder. This indicates that the sintering temperature should be controlled below the critical temperature of 1150 °C. Fig. 4d shows the voltage profiles of the electrodes sintered at 1100 and 1125 °C. Note that it was not possible to fabricate the sintered electrode at 1150 °C because of melting, as shown in Fig. 4e. The electrode sintered at 1100 °C shows compatible charge and discharge capacity of 159.6 and 155.7 mAh/g, respectively, while the electrode sintered at 1125 °C shows only 127.2 mAh/g, which is a 18 % reduction of discharge capacity compared to sintering at 1100 °C. This loss of capacity may be a result of the partial transformation of LCO to Co_3O_4, as confirmed by XRD. Fig. 4e and 4f show SEM images of LCO sintered at 1150 °C and 1100 °C, respectively, indicating melted particles at 1150 °C. However, the electrode at 1100 °C revealed a well-sintered particle without any abnormal melted microstructure, as

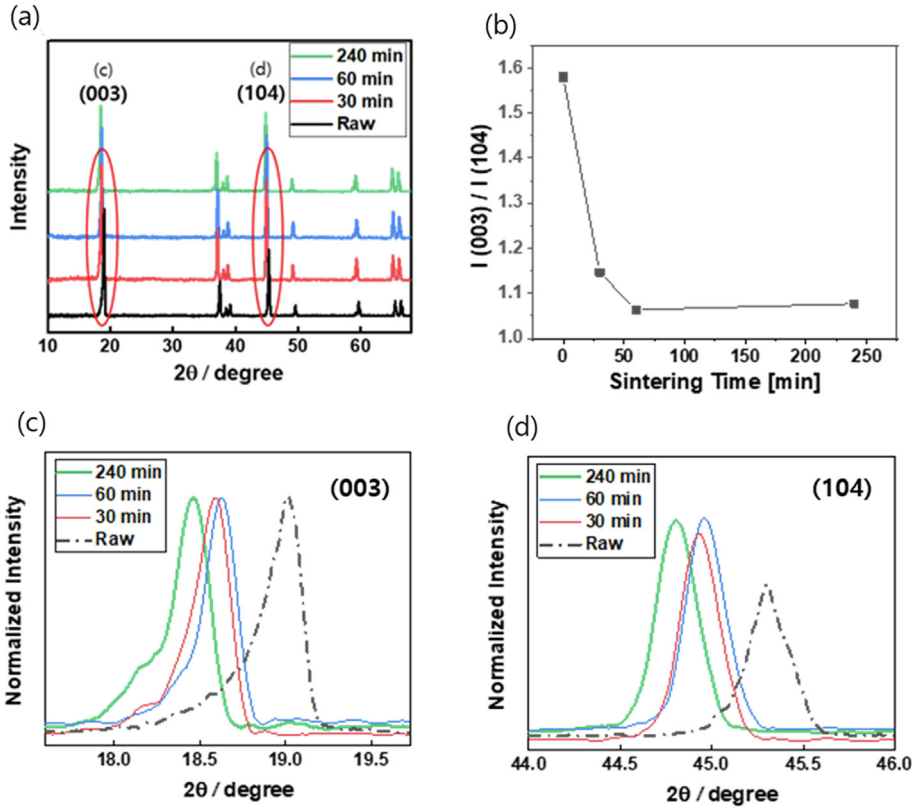

Fig. 5. (a) X-ray diffraction patterns for different sintering time sintered at 1100 °C, (b) I (003) / I (104) ratio indicating cation mixing phase as increased sintering time, and (c,d) X-ray diffraction patterns of (003) and (104) planes.

shown in Fig. 4f. Both oxygen evolution and phase decomposition are associated with the sintering conditions; therefore, the temperature was set to 1100 °C to fabricate a high-performance sintered LCO electrode because the structural stability is sensitive to the electrochemical performance.

The structural stability of the LCO electrodes, sintered at different holding times from 30 to 240 min at 1100 °C, was investigated using XRD patterns and lattice parameters. Compared to the raw powder, as shown in Fig. 5a, all sintered LCO electrodes also possess well-defined major diffraction peaks of (003) and (104). The diffraction patterns represent rhombohedral symmetry with the space group of R $\bar{3}$ m without any impurity peaks of CoO or Co_3O_4, thereby indicating no structural instability in the layered structure of LCO after sintering. Table 1 shows that the average lattice parameters and c/a ratio calculated from the XRD patterns are a = 2.83 ± 0.02, c = 14.20 ± 0.19 nm, and 5.02, respectively, which match well with the parameters reported in the reference LCO [21,22].

Observations, shifts, and intensity ratios in the diffraction peaks of the (003) and (104) planes, as shown in Fig. 5c and 5d, were discovered from the LCO electrodes sintered at 1100 °C for different holding times. A peak shift of 0.5 °was observed in the electrode sintered for 240 min, indicating an increase in the d-spacing in the Li layer. The correlation between the sintering time and intensity ratio is shown in Fig. 5b, showing a decrease in the ratio of the diffraction peaks from 1.580 to 1.077. This is closely associated with cation mixing, as shown in Fig. 6. Conventional LCO materials have well-ordered structures such that cobalt transition metal (TM) and Li ions are alternatively located in the TM sites and Li layers of the (104) planes, but Li ions are only located at the Li layers of the (003) planes [23]. However, Fig. 5b displays the partial cation mixing detected in the sintered LCO electrode such that Co ions migrate into the octahedral sites of the Li layers, thus

Table 1
Lattice parameters of sintered $LiCoO_2$.

Sintering time [min]	Lattice parameters		c/a
	a [Å]	c [Å]	
0	2.806	13.932	4.9649
30	2.836	14.328	5.0516
60	2.834	14.291	5.0423
240	2.846	14.421	5.0670

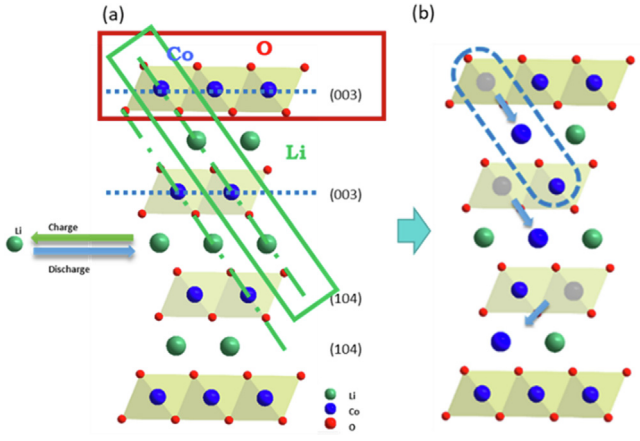

Fig. 6. Crystal structure illustration of (a) well-ordered $LiCoO_2$ and (b) partially cation mixed $LiCoO_2$ with occupied Co ions in Li layer.

resulting in a large intensity of the (104) plane and a decrease in the intensity ratio to 1.077.

3.3. Densification and coarsening behaviors

The electrochemical performance of the sintered electrode is dependent on the microstructure and key factors directly related to Li-ion conduction. For instance, small grains not only afford a higher power density with a shorter Li-ion diffusion length, but also a denser structure that enhances the energy density by storing more Li ions [24]. To investigate the sintering behavior of LCO, microstructural evolutions, such as relative density and grain size, were classified as densification and coarsening mechanisms in accordance with different sintering environments.

Fig. 7a shows microstructures and particle size distribution of sintered LCO electrodes according to different sintering times at 1100 °C. Significant grain growth was not observed for the short sintering times of 15 and 45 min compared to the raw LCO particles of 3.5 μm. In contrast, at longer sintering times of up to 240 min, the grain size greatly increased to 8.37 μm in the range of 4–14 μm. Fig. 7b displays the percentage cumulative frequency of the particle size with increasing sintering time. The cumulative percentage shows that 80 % of particles, sintered for 240 min, increased to sizes bigger than 10 μm. The grain size increased rapidly during the sintering process at 1100 °C, as shown in Fig. 7c. Even for short periods of 15 and 45 min at stage I, grain sizes were similar to raw particles, but densification rapidly increased to 73 % by the neck growth associated with surface energy at the vapor–solid interfaces. This indicates that bulk transport mechanisms of grain boundary and volume diffusion are dominated as seen in Fig. 8d [25]. Meanwhile, sintering for 240 min in stage II showed sluggish densification with monotonous increment of 2.5 %/h, but grain sizes greatly increased to 8.37 μm which led to isolated pores breaking away from the grain boundaries, as well as a penalty for the Li-ion conduction due to the slow Li-ion diffusivity of 10^{-10} cm^2/sec in the grain [26].

Despite of holding long sintering time, the maximum relative density achieved was only 85.3 % owing to the additives such as carbon black and a binder of 10 vol% that were added to the green bodies of electrodes. The additives were eliminated at approximately 600 °C during the thermal process and were transformed into a porous structure. After filling with a solid electrolyte, the structure will have less tortuous and interconnected pathways for Li-ion transport, which will facilitate fast Li-ion conductivity and facilitate the development of high power and energy densities in all-solid-state batteries [27]. From a practical point of view, maximizing the energy and power densities of solid-state batteries is required when considering how to design dense structures with small grain sizes by understanding the mechanisms of densification and coarsening behavior.

To control the grain growth and understand the correlation between the grain size and sintering temperature, the kinetics of the grain growth were studied at different sintering temperature from 1000 °C to 1125 °C as shown in Fig. 8. Densification and coarsening were not observed at the temperature lower than 1000 °C as shown in Fig. s1, therefore, kinetics study was conducted in the temperature range of 1000 °C to 1125 °C. It is shown that grain growth is highly temperature-dependent. The grain size of d50 increased from 3.4 μm to 8.7 μm at 1100 °C, while it increased to 24.6 μm at 1125 °C as represented in Fig. 9(a-c). Fig. 9d illustrates the activation energies for grain growth obtained from the relationship between the log plot of the average grain size and sin-

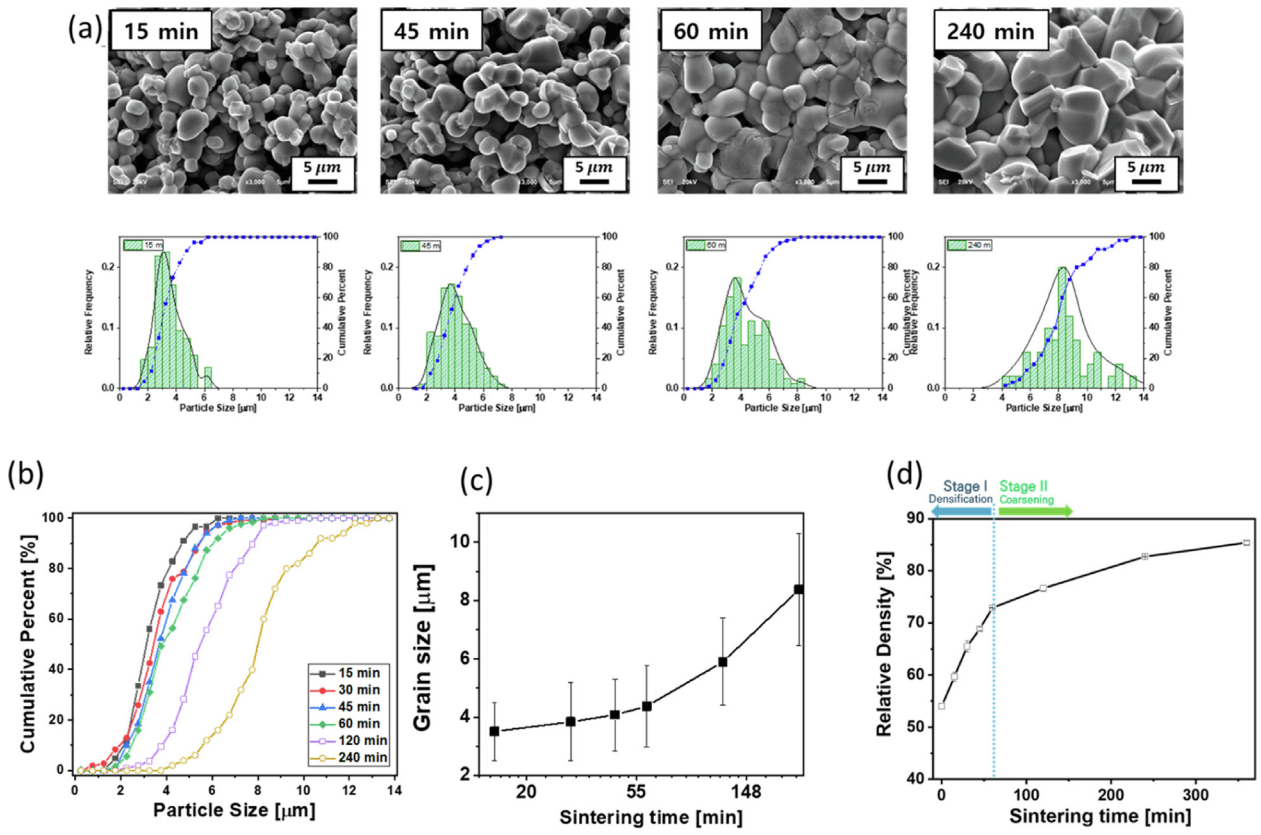

Fig. 7. Comparison of microstructure as increased sintering time from 15 to 240 min (a) SEM images with normalized grain size histograms, (b) cumulative percent as function of particle size, (c) grain size and (d) changes in relative density at two different stages.

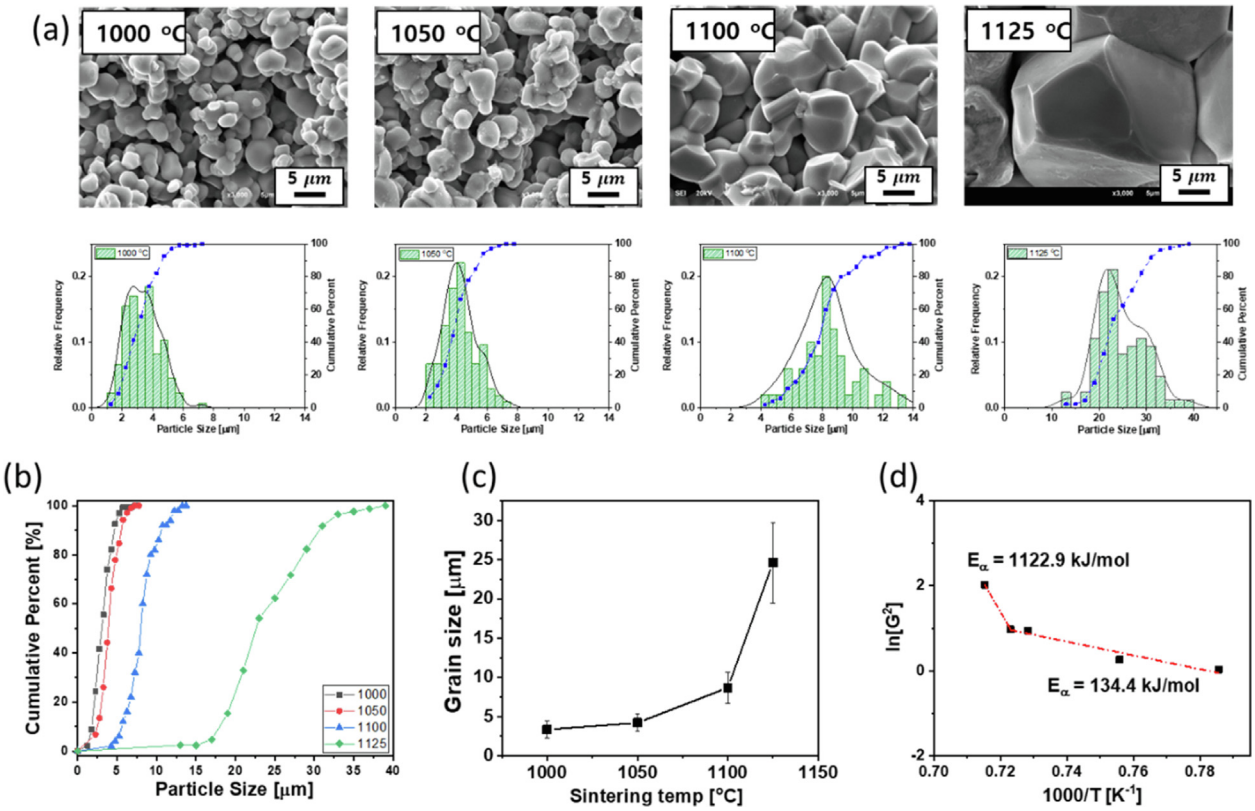

Fig. 8. Comparison of microstructure as increased sintering temperature from 1000 to 1125 °C (a) SEM images with normalized grain size histograms, (b) cumulative percent as function of particle size, (c) grain size and (d) grain growth kinetics for LCO with activation energies.

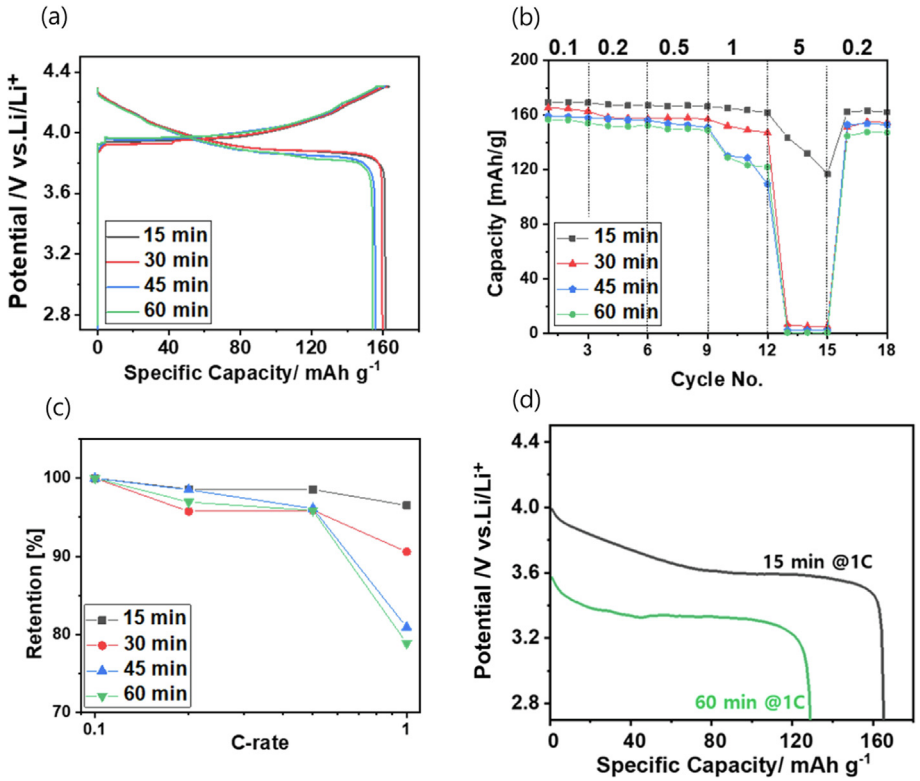

Fig. 9. Electrochemical characterization of 150 μm -thick electrodes fabricated by sintering (a) First charge and discharge curves at the low c-rate of 0.1C, (b) Specific discharge capacity versus C-rate, (c) Rate retention and (d) First discharge curves obtained from 15 and 60 min sintered electrode at the high c-rate of 1C.

tering temperature. The calculated slope indicates the activation energy for grain growth according to the grain coarsening equation [28].

$$G^n - {G_0}^n = k_0 \exp\left(\frac{-E_a}{kT}\right)t$$

where G is the average grain size at a certain time (t), G_0 is the initial grain size, n is the grain growth exponent, E_a is the activation energy for grain growth, R is the gas constant, T is the absolute temperature, and k_0 is an empirically derived proportionality constant. The n value of 2, showing a well fit as seen in Fig. 8d, is usually associated with normal grain growth without secondary phases or impurities, which can result in sluggish mobility of the grain boundaries [29]. The slope dramatically changed near 1110 °C, which denotes a change in the activation energy from 636 to 1470 kJ/mol for grain growth, indicating two distinct stages representing the intermediate and final stages of the sintering process [30]. In general, rate-limiting species are the slowest moving ions through the lattice or grain boundaries because of their large size for grain growth in ceramics [31]. In the case of LCO, the oxygen anion with the largest radius of 140 pm is expected to be the main rate-controlling species, and this correlates with the activation energy for grain growth. The activation energy of LCO has never been reported so far; however, 636 kJ/mol is similar to that reported for ceramics.

3.4. Correlation between microstructures and electrochemical properties

Galvanostatic charge and discharge techniques were used to investigate the correlations between electrochemical performance and microstructures. The sintered electrodes in the densification region from 15 min to 60 min were evaluated using a coin-type cell (CR2032) with a thickness of 150 μm. Fig. 9a shows the voltage profiles of the sintered electrodes during the first charge and discharge. All electrodes sintered at 1100 °C at the region with relative density from 54 to 72.9 % showed the similar specific capacities of 160 mAh/g at a slow c-rate of 0.1C. The charge and discharge performances were compatible with those of conventional Li-ion batteries, where highly densified sintered LCO can be considered as a candidate for ASSB electrodes. Even though grain size and relative density increased to 4.4 μm and 72.9 %, respectively, after sintering for 60 min, no transport problem of Li-ions existed in sintered LCO electrodes. Furthermore, the discharge capacity of 160 mAh/g, which is very close to the practical capacity of LCO, indicates that there was enough electrolyte infiltrated into the highly densified sintered electrode. Li ions easily diffused through larger grains without any binder or conductive material, representing an insignificant effect of sintering durations ranging from 15 to 60 min on the discharge capacities at 0.1C rate.

To better understand the effect of microstructures on Li ion diffusion at a fast C-rate, the rate performances of the sintered LCO electrodes were studied as a function of the high discharge rate, as shown in Fig. 9b-d. The result reveals dramatic capacity fading as the sintering time increases, resulting in a larger grain size and higher density. At the low c-rates of 0.1C and 0.2C, all sintered electrodes exhibited similar rate capabilities, but their rate capabilities were significantly distinguishable at current densities of 0.5 and 1C. The rate retentions at 1C were 96.5, 90.6, 80.9, and 78.9 %, respectively, and a sintering time longer than 45 min showed a significantly decreased rate capability, indicating poor Li-ion diffusion with a grain size larger than 4.0 μm and relative density higher than 68.9 %. Furthermore, the electrode sintered for 60 min suffered from large polarization, leading to a dramatic potential drop due to sluggish Li-ion conduction in the sintered electrode; thus, the discharge capacities significantly decreased from 154 to 129 mAh/g, as shown in Fig. 9d.

As shown in Fig. 1, the diffusion paths are categorized into three parts: diffusion in the crystal, diffusion from one primary to another, and diffusion into pores. Among these three diffusions, the conduction in the crystal was negligible because a well-maintained layered structure was confirmed, and significant structural differences were not observed using XRD compared to the dramatic change in grain size and relative density. However, diffusion within the grain is directly related to grain growth and diffusion at the grain boundary, and diffusion path refer to tortuosity. Hence, the grain size, number of grain boundaries, and tortuosity were used for the calculation, and the parameters for the diffusion model are listed in Table 2. Given an electrode thickness of 150 μm, the effective diffusion length depends on the tortuosity at different sintering times. As increased sintering time from 15 to 60 min, the effective diffusion length increased from 354.3 μm to 432.2 μm, giving rise to an escalated tortuosity from 2.36 to 2.88. Additionally, the grain growth is considered to be the effective diffusivity (D_{eff}) at different sintering times, as illustrated in Fig. 10a. D_{eff} decreases from 5.02×10^{-7} to 3.18×10^{-7} cm^2/sec as the grain size increases owing to lower D_b as shown in Fig. s2, resulted in sluggish lithium ion diffusion in larger grain size. To verify the effects of tortuosity and grain size on Li diffusion, the calculated rate capability at 1C was compared with the experimental results, as shown in Fig. 10b. The calculated rate retention showed 100 % retention at sintering times up to 30 min, whereas experimental results showed 91 % retention sintering for 30 min. This might be due to the lack of electrical conductivity of the sintered electrode because conductive materials such as additional carbon black were not added to investigate pure LCO behavior in this study. When the LCO electrode was sintered for 45 and 60 min, the calculated retention was consistent with the experimental results, thus verifying our assumption of tortuosity and the grain size effect on Li diffusion with increasing sintering time. In addition, the maximum c-rate limit was calculated, as shown in Table 2, indicating that the sintered electrode had full retention at 1.43, 1.03, 0.82, and 0.61, respectively. These findings are consistent with the experimental rate properties. This maximum c-rate for full retention shows slightly higher value than experimental value of 1C for the same reason mentioned above. It is believed that adding conductive materials after sintering to increase the electrical conductivity can reduce the gap between the calculated and experimental results. Consequently, the increased tortuosity and reduced surface in the densified cathode, which lead to a longer diffusion path and lower diffusivity, are the main rate-limiting parameters in sintered electrodes. Therefore, Li-ion facilitating can be achieved by heat

Table 2
Parameters used in diffusion model of sintered $LiCoO_2$.

Sintering time [min]	Relative density [%]	Tortuosity	Diffusion length [μm]	X_{gb}	X_g	D_{eff} [cm^2/sec]	C-rate limit
0	59.68	2.3623	354.3	0.5000	0.5000	5.02×10^{-7}	1.438
30	65.47	2.5527	382.9	0.4190	0.5810	4.20×10^{-7}	1.031
60	68.85	2.6876	403.1	0.3696	0.6304	3.70×10^{-7}	0.819
240	72.90	2.8814	432.2	0.3179	0.6821	3.18×10^{-7}	0.613

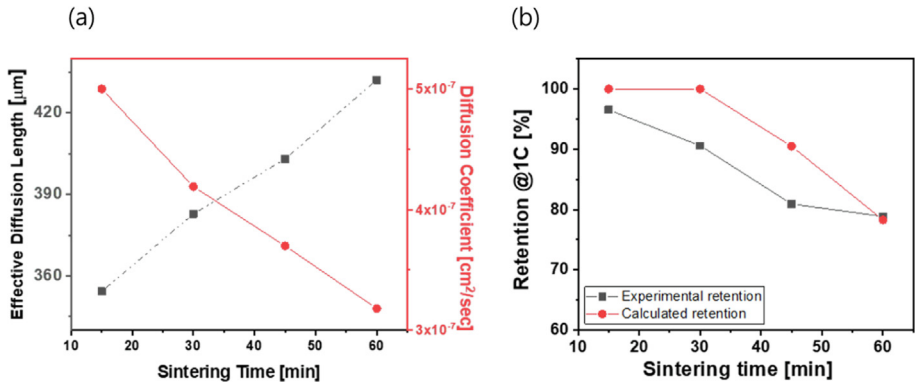

Fig. 10. (a) Effective diffusion length and diffusion coefficient and (b) Comparison between experimental and calculated result of rate retention versus sintering time.

treatment at the dominant region of densification without rapid grain growth.

4. Conclusions

In summary, we demonstrated highly densified LCO by sintering to tailor diffusion length and diffusivity based on densification and coarsening under various sintering condition. The correlation between the microstructure and Li-ion diffusion in densified electrode was studied in terms of the thermal stability, densification behavior, and electrochemical performance. The thermal stability results suggest a transformation to a nonstoichiometric phase with Co_3O_4 in the sintered electrode exposed to temperatures higher than the critical temperature of 1154 °C. However, the electrode sintered at 1100 °C showed a well-maintained layered structure without any second phase or impurity. The relative density of LCO significantly increased in two distinct stages, and the activation energies were 636 and 1470 kJ/mol for grain growth, which can be used for electrode design by heat treatment. The rate performance indicated a notably decreased retention with a longer sintering time. It is believed that this degradation resulted from the large grain size and increased tortuosity owing to densification, indicating stable and fast diffusion can be achieved without coarsening by heat treatment less than the critical point of 1154 °C. Such information, combined with sintering behavior with kinetic study and electrochemical properties of diffusion, may help in the design of densified cathodes, which is a cost-effective process for fabricating high-performance cathodes.

Data availability

The data that has been used is confidential.

Declaration of Competing Interest

The authors declare that they have no known competing financial interests or personal relationships that could have appeared to influence the work reported in this paper.

Acknowledgements

This research was supported by the Korea Institute for Advancement of Technology (KIAT) grant funded by the Ministry of Trade, Industry and Energy (Grant P0016145 and P0019231) and the frameworks of Global Joint Research Promotion Program managed by the National Research Council of Science and Technology (NST, Grant No. NST-02) of the Ministry of Science and ICT (MSIT) and the International Cooperative Project of CAS (No.122111KYSB20210012).

Appendix A. Supplementary material

Supplementary data to this article can be found online at https://doi.org/10.1016/j.matdes.2023.111695.

References

[1] J.M. Tarascon, M. Armand, Issues and challenges facing rechargeable lithium batteries, Nature 414 (6861) (2001) 359–367.
[2] C. Sun, J. Liu, Y. Gong, D.P. Wilkinson, J. Zhang, Recent advances in all-solid-state rechargeable lithium batteries, Nano Energy 33 (2017) 363–386.
[3] H.S. Santos, R. Sliz, H. Nguyen, S. Srivastava, D. Ramteke, T. Fabritius, U. Lassi, P. Kinnunen, Hybrid amorphous-crystalline silicate composites as feasible solid-state electrolytes, Mater. Des. 217 (2022) 110599.
[4] J. He, L. Zhang, L. Liu, Improving thermal conduction across cathode/electrolyte interfaces in solid-state lithium-ion batteries by hierarchical hydrogen-bond network, Mater. Des. 194 (2020) 108927.
[5] P.-Y. Yen, M.-L. Lee, D.H. Gregory, W.-R. Liu, Optimization of sintering process on Li1+xAlxTi2-x(PO4)3 solid electrolytes for all-solid-state lithium-ion batteries, Ceram. Int. 46 (12) (2020) 20529–20536.
[6] J.-H. Seo, J. Guo, H. Guo, K. Verlinde, D.S.B. Heidary, R. Rajagopalan, C.A. Randall, Cold sintering of a Li-ion cathode: LiFePO4-composite with high volumetric capacity, Ceram. Int. 43 (17) (2017) 15370–15374.
[7] S. Ohta, J. Seki, Y. Yagi, Y. Kihira, T. Tani, T. Asaoka, Co-sinterable lithium garnet-type oxide electrolyte with cathode for all-solid-state lithium ion battery, J. Power Sources 265 (2014) 40–44.
[8] L.-L. Lu, Y.-Y. Lu, Z.-J. Xiao, T.-W. Zhang, F. Zhou, T. Ma, Y. Ni, H.-B. Yao, S.-H. Yu, Y. Cui, Wood-Inspired High-Performance Ultrathick Bulk Battery Electrodes, Adv. Mater. 30 (20) (2018) 1706745.
[9] S. Yamakawa, S. Ohta, T. Kobayashi, Effect of positive electrode microstructure in all-solid-state lithium-ion battery on high-rate discharge capability, Solid State Ion. 344 (2020) 115079.
[10] S. Han, J. Park, W. Lu, A.M. Sastry, Numerical study of grain boundary effect on Li+ effective diffusivity and intercalation-induced stresses in Li-ion battery active materials, J. Power Sources 240 (2013) 155–167.
[11] M. Park, X. Zhang, M. Chung, G.B. Less, A.M. Sastry, A review of conduction phenomena in Li-ion batteries, J. Power Sources 195 (24) (2010) 7904–7929.
[12] Y. Dong, H. Yang, L. Zhang, X. Li, D. Ding, X. Wang, J. Li, J. Li, I.-W. Chen, Ultra-Uniform Nanocrystalline Materials via Two-Step Sintering, Adv. Funct. Mater. 31 (1) (2021) 2007750.
[13] S. Sharifi-Asl, J. Lu, K. Amine, R. Shahbazian-Yassar, Oxygen Release Degradation in Li-Ion Battery Cathode Materials: Mechanisms and Mitigating Approaches, Adv. Energy Mater. 9 (22) (2019) 1900551.
[14] S. Sharifi-Asl, F.A. Soto, A. Nie, Y. Yuan, H. Asayesh-Ardakani, T. Foroozan, V. Yurkiv, B. Song, F. Mashayek, R.F. Klie, K. Amine, J. Lu, P.B. Balbuena, R. Shahbazian-Yassar, Facet-Dependent Thermal Instability in LiCoO2, Nano Lett. 17 (4) (2017) 2165–2171.
[15] E. Antolini, M. Ferretti, Synthesis and Thermal Stability of LiCoO2, J. Solid State Chem. 117 (1) (1995) 1–7.
[16] D. Mohanty, J. Li, D.P. Abraham, A. Huq, E.A. Payzant, D.L. Wood, C. Daniel, Unraveling the Voltage-Fade Mechanism in High-Energy-Density Lithium-Ion Batteries: Origin of the Tetrahedral Cations for Spinel Conversion, Chem. Mater. 26 (21) (2014) 6272–6280.
[17] K. Kleiner, B. Strehle, A.R. Baker, S.J. Day, C.C. Tang, I. Buchberger, F.-F. Chesneau, H.A. Gasteiger, M. Piana, Origin of High Capacity and Poor Cycling Stability of Li-Rich Layered Oxides: A Long-Duration in Situ Synchrotron Powder Diffraction Study, Chem. Mater. 30 (11) (2018) 3656–3667.

[18] K. Kang, G. Ceder, Factors that affect Li mobility in layered lithium transition metal oxides, Phys. Rev. B 74 (9) (2006) 094105.
[19] D. Eum, B. Kim, S.J. Kim, H. Park, J. Wu, S.-P. Cho, G. Yoon, M.H. Lee, S.-K. Jung, W. Yang, W.M. Seong, K. Ku, O. Tamwattana, S.K. Park, I. Hwang, K. Kang, Voltage decay and redox asymmetry mitigation by reversible cation migration in lithium-rich layered oxide electrodes, Nat. Mater. 19 (4) (2020) 419–427.
[20] H. Gao, Q. Wu, Y. Hu, J.P. Zheng, K. Amine, Z. Chen, Revealing the Rate-Limiting Li-Ion Diffusion Pathway in Ultrathick Electrodes for Li-Ion Batteries, J. Phys. Chem. Lett. 9 (17) (2018) 5100–5104.
[21] R.J. Gummow, M.M. Thackeray, W.I.F. David, S. Hull, Structure and electrochemistry of lithium cobalt oxide synthesised at 400°C, Mater. Res. Bull. 27 (3) (1992) 327–337.
[22] Y.-M. Choi, S.-I. Pyun, S.-I. Moon, Effects of cation mixing on the electrochemical lithium intercalation reaction into porous Li1 − δNi1 − yCoyO2 electrodes, Solid State Ion. 89 (1) (1996) 43–52.
[23] A. Abdellahi, A. Urban, S. Dacek, G. Ceder, Understanding the Effect of Cation Disorder on the Voltage Profile of Lithium Transition-Metal Oxides, Chem. Mater. 28 (15) (2016) 5373–5383.
[24] H. Jeong, S.-J. Lim, S. Chakravarthy, K.H. Kim, J. Lee, J.S. Heo, H. Park, Three-dimensional cathode with periodically aligned microchannels for improving volumetric energy density of lithium-ion batteries, J. Power Sources 451 (2020) 227764.
[25] R.L. Coble, Sintering Crystalline Solids. I. Intermediate and Final State Diffusion Models, J. Appl. Phys. 32 (5) (1961) 787–792.
[26] R.M. German, 1 - Thermodynamics of sintering, in: Z.Z. Fang (Ed.), Sintering of Advanced Materials, Woodhead Publishing, 2010, pp. 3–32.
[27] C.-J. Bae, C.K. Erdonmez, J.W. Halloran, Y.-M. Chiang, Design of Battery Electrodes with Dual-Scale Porosity to Minimize Tortuosity and Maximize Performance, Adv. Mater. 25 (9) (2013) 1254–1258.
[28] T. Senda, R.C. Bradt, Grain Growth in Sintered ZnO and ZnO-Bi2O3 Ceramics, J. Am. Ceram. Soc. 73 (1) (1990) 106–114.
[29] A. Sharafi, C.G. Haslam, R.D. Kerns, J. Wolfenstine, J. Sakamoto, Controlling and correlating the effect of grain size with the mechanical and electrochemical properties of Li7La3Zr2O12 solid-state electrolyte, J. Mater. Chem. A 5 (40) (2017) 21491–21504.
[30] W. Huddleston, F. Dynys, A. Sehirlioglu, Effects of microstructure on fracture strength and conductivity of sintered NMC333, J. Am. Ceram. Soc. 103 (3) (2020) 1527–1535.
[31] R.S. Gordon, Mass Transport in the Diffusional Creep of Ionic Solids, J. Am. Ceram. Soc. 56 (3) (1973) 147–152.